Supporting Information

# Untethered actuation of hybrid hydrogel gripper via ultrasound

*Hyegyo Son[#†], Eunjeong Byun[#‡], Yeon Ju Yoon[†], JuHong Nam[‡], Seung Hyun Song[*‡†] &*

*ChangKyu Yoon[*†]*

H. Son, Y. J. Yoon, Prof. C. K. Yoon
[†]Department of Mechanical Systems Engineering, Sookmyung Women's University, Seoul, 04310, South Korea.
[†]Institute of Advanced Materials and Systems, Sookmyung Women's University, Seoul, 04310, South Korea.
*Email: ckyoon@sookmyung.ac.kr

E. Byun, J. Nam, Prof. S. H. Song
[‡]Department of Electronics Engineering, Sookmyung Women's University, Seoul, 04310, South Korea.
[†]Institute of Advanced Materials and Systems, Sookmyung Women's University, Seoul, 04310, South Korea.
*Email: shsong.ee@sookmyung.ac.kr

*Corresponding author
[#]Equal contribution

## Table of contents

## Materials

Acrylamide (AAM, Sigma-Aldrich), *N*-isopropyl acrylamide (NIPAM, Sigma-Aldrich), Poly-*N*-isopropylacrylamide (pNIPAM, Sigma Aldrich), Laponite XLG (BYK), 2-Hydroxy-4'-(2-hydroxyethoxy)-2-methylpropiophenone (Irgacure 2959, Sigma Aldrich), Rhodamine 6G (Sigma Aldrich), *N*, *N*'-methylenebisacrylamide (BIS, Sigma Aldrich), Iron(III) Oxide red ($Fe_2O_3$, DUKSAN general science), N, N, N-tetramethylethylenediamine (TMEDA, Sigma Aldrich), Ammonium sulfate (APS, Sigma Aldrich), Fluorescein O-methacrylate (Sigma Aldrich), and Sodium hydroxide beads (NaOH, Sigma Aldrich) were used as received.

## Note S1. Preparation of NIPAM, AAm and ferrogels

The stimuli responsive shape-changing soft robots have mostly been implemented in the form of two-dimensional (2D) thin films using photolithography so far.[1,2] Inhomogeneous structures like thin bilayer or bi-stripe composed of different swelling-and-deswelling powers between layers are primarily considered to create shape transformation of soft robots.[3] Although those thin bilayer or bi-stripe structures are enabled to fold, bend, or roll themselves like paper origami, those shape changes or movement in 3D is limited since it is a combination of 2D structures. One of the alternatives to overcome the geometric design limitations is a 4D printing that can introduce time-dependent 3D shape-changing hydrogel devices[4–7] which incorporates various fabrication methodological strategies such as top-down lithography, molding, and printing.

In this regard, 3D printable NIPAM and AAm pre gel inks were prepared by tuning a previously published method.[8] In brief, for ultrasound responsive NIPAM-based gel ink, NIPAM, pNIPAM, and Irgacure 2959 were mixed in DI water by using a magnetic stirrer for 24 hours until diluted completely. Then, Laponite XLG, and Rhodamine 6G were vortexing at least 6 hours. The Rhodamine 6G was particularly prepared for dying NIPAM-based gel to obtain clear optical and fluorescence images. After mixing thoroughly, the ultrasound responsive gel ink was transferred into a 3D printing cartridge by using a syringe. Specific weights of ultrasound responsive gel ink per 20 mL solution were as follows: 1.692 g NIPAM, 0.02 g pNIPAM, 1.354 g Laponite XLG, 0.034 g Irgacure, 0.1 mg Rhodamine 6G, and 16.92 g DI water. For stimuli non-responsive AAm-based structural gel ink, AAm and BIS were dissolved in DI water by using a magnetic stirrer for 24 hours until diluted completely. Then, Laponite XLG and Fluorescein O-methacrylate dye were mixed thoroughly at least for 6 hours. By following the same way as preparation of ultrasound responsive gel ink, the solution was transferred into another empty cartridge. The specific weights of structural gel ink per 20 mL solution were as follows: 1.576 g AAm, 0.332 g BIS, 1.328 g Laponite XLG, 0.166 g Irgacure, 0.1 mg NaOH, 0.1 mg Fluorescein O-methacrylate, and 16.594g DI water.

Furthermore, we used $Fe_2O_3$-pAAm gel (Ferrogel) for control of the magnetic field by neodymium magnet. Two solutions (A and B) consisted of $Fe_2O_3$ and ammonium persulfate (APS) respectively.[9] In detail, the recipe for solution A was as follows (wt %): AAm (71 %), BIS (3.5 %), and $Fe_2O_3$ (25.5 %) in 1.2 ml of DI water with 10 μl of TMEDA accelerator. Also, the recipe for solution B was 80 mg/ml of APS. We mixed solution A and B in a 40:1 ratio in ferrogel with a polymerization time of 20 sec. Polymerization time can be increased by reducing the concentration of the accelerator.

**Note S2. 3D printing NIPAM and AAm pre-gel inks**

We used the direct dual ink writing 3D bioprinter (Inkredible$^{+}$, Cellink). All 3D hydrogel structures were designed using the auto computer-aided-design (AutoCAD) software and generated STL files for recognizing the dual hydrogel modules in 3D bioprinter. Then, dual ultrasound responsive and structural pre-gels' print paths were generated via G-code which outputs the XYZ motion of the two print heads using the Slic3r software with a layer height of 0.4 mm with printing speed 10 mm $s^{-1}$, infill density 60~65 %, and printing pattern of rectilinear. After the 3D printing process, we photocured the 3D structures using a 365 nm wavelength UV light source chamber (BLX, Bio-Link). We cured the structures for 4 min 30 sec in all directions at the same time. The intensity of the UV light was 4.9 mJ/sec.

In specific, the inner layer was set as an ultrasound responsive layer for shrinking when the temperature was increased, and the outer layer was set as a structural layer. We put a support structure inside of the whole structure for maximizing actuation and holding the legs of our gripper. It consisted of ultrasound responsive NIPAM-based gel. The ratio between the ultrasound and structural layers was 2:1. In the structural layer, there was a long and thin hole for $Fe_2O_3$-pAAm gel injection after 3D printing. The width of the hole was 2 mm. Also, we applied an offset between the ultrasound responsive and structural layer as a 1 mm width because there was a calibration error in small quantities, in a 3D printing process.

Dual NIPAM-based and AAm-based gels printing required several challenges to be overcome. Two materials were needed to be aligned during switching materials without seamless. Even a small misalignment between two nozzles resulted in significant accumulation errors in the final structure. Thus, any misalignments were observed, we changed the preset positioning g-code values in the X and Y directions and this step was repeated until the dual print heads were perfectly aligned having continuous printing of the two inks. In addition, it was critical to set an offset (Z direction) of the starting point of each ink to be aligned perfectly. Thus, the positioning calibration including Z direction height was double checked at every printing step.

We made sure that both print heads were leveled with each other in the Z direction. Then, for calibration in the X and Y directions, we printed a calibration structure consisting of a NIPAM-based gel on top of an AAm-based gel. The objective of this step was to check whether there was any misalignment between the two print heads because even a small misalignment will accumulate recurring errors in each layer, resulting in defects in the structure and undesired shape change. If any misalignments were observed, we added preset values in the X and Y directions for the print heads in the g-code files. This step was repeated multiple times until the print heads were perfectly aligned to ensure the seamless printing of the two inks.

**Note S3. Optimization of 3D printing parameters**

To find the optimal 3D printing parameters, we tested different combinations of printing pressure, print speed, nozzle diameters, and ink composition. We found that the viscoelastic properties of the ink, determined by the weight ratio of the sheer thinning agent, are the most significant parameters with respect to the precise 3D printing and UV curing processes. In particular, the rest of the printing parameters are heavily affected by ink viscoelasticity. Thus, we firstly optimized the weight ratio of the Laponite XLG intensively to precisely develop 3D printable gels that have appropriate viscoelastic properties. We found that the weight ratio of the sheer thinning agents (Laponite XLG) is critical; if the weight ratio was too high, it became difficult to print within the appropriate pressure range (10~100 kPa). Similarly, if the weight ratio was too low, the 3D printed structures collapsed before the UV curing process. Consequently, we set the weight percent of Laponite XLG to be 6.8 % in the NIPAM-based and AAm-based inks. Furthermore, under this fixed shear-thinning agent ratio, we optimized the printing pressures of the ultrasound responsive and structural gels for the printing speed of 10 mm $s^{-1}$.

We printed 12 layers of gripper structures for both ultrasound responsive and structural gels. As discussed in the Figure 2B-E of the main text, the fabrication process can be divided into 4 steps (Figure S1A-D). The structural gel was printed first, then the ultrasound responsive gel was printed. Particularly, the ultrasound responsive layers consisted of the leg and carrier parts of the hybrid gripper. First, the legs and carrier parts were printed together for two layers. (Figure S1B). One layer was extruded for 0.4 mm heights. Then, the rest of gripper legs was printed (Figure S1C). The printing pressures and nozzle tips were 20-30 kPa and 0.21 mm for ultrasound responsive gels and 60-70 kPa and 0.41 mm for structural gels respectively. In addition, we observed significant differences in printing pressures according to the types of nozzle tips (Figure S1E). When the stainless-type nozzle tip was used, the printing pressure was 20~30 kPa higher than that of the plastic-type nozzle tip. Furthermore, the layouts and dimensions of the hybrid gripper are described in Figure S1F&G. The ratio of thickness between structural layer and ultrasound responsive layer was decided as 1:2 (1.5 mm and 2.7 mm) based on the bending data described in Figure 2H.

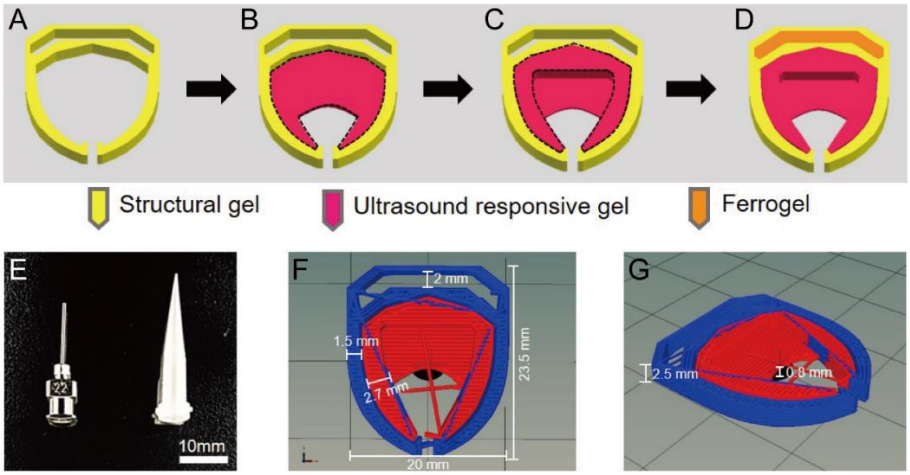


**Figure S1**. **Details about optimization of 3D printing a hybrid gripper. (A-D)** Schematics showing the steps of 3D printing structural gel, ultrasound responsive gel, and magnetic responsive ferrogel in order. **(E)** Different printing nozzle tips for structural gel printing (stainless-type, left) and for ultrasound responsive gel printing (plastic-type, right). **(F, G)** Layouts and dimensions of the hybrid gripper. Scale bar (E) indicates 10 mm.

**Note S4. Characterization of swelling ratio (NIPAM-based and AAm-based gels)**

We verified the swelling-deswelling of the stimuli responsive NIPAM-based and stimuli non-responsive AAm-based gels. We printed each disk-shaped thin NIPAM-based and AAm-based gels and observed the swelling-deswelling power in DI water by measuring the diameter changes at different temperature ranges (Figure S2). Before measuring the swelling ratio, all samples were allowed to reach an equilibrium state at least 24 hours in DI water (Figure S2A). We observed an increase in the diameter (39 %) of the 3D printed NIPAM-based disk-shaped gel with no diameter changes of AAm-based gel (Figure S2B). This swelling of NIPAM-based and non-swelling AAm-based gels agrees with prior swelling data.[10] Further, it is well known that the NIPAM gel network demonstrates a sharp critical transition point of low critical solution temperature (LCST) that exhibits hydrophilic swelling (below LCST) and hydrophobic deswelling (above LCST) properties between 32 °C and 37 °C.[11,12] Consequently, we considered the NIPAM-based gel as the ultrasound responsive gel that drives shape deformation by swelling-deswelling, while the AAm-based gel does not display any shape changes.

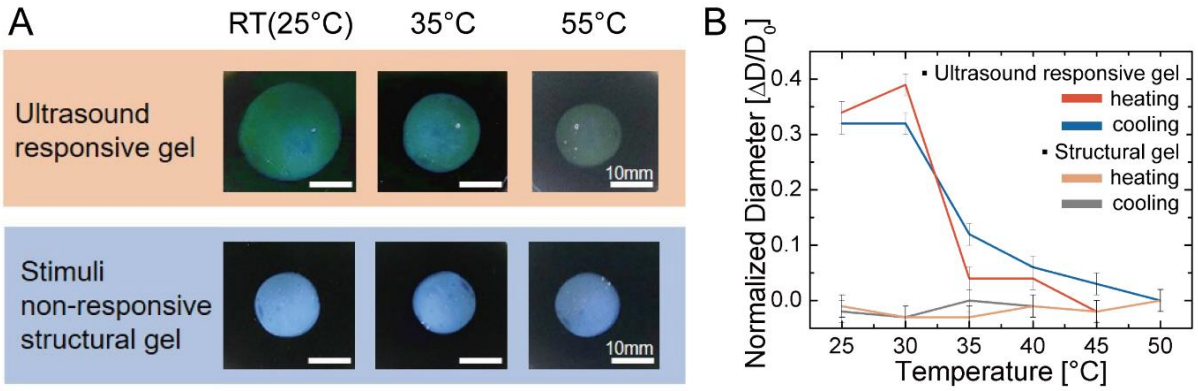


**Figure S2**. **Experimental characterization of the swelling of printed ultrasound-responsive and structural hydrogel structures. (A)** Figures showing the state of ultrasound responsive and structural disk-shaped gel at RT (25 °C), 35 °C, and 55 °C, respectively. Scale bars mean 10 mm. **(B)** Plot showing the experimentally measured normalized diameter change in DI water at different temperatures between RT and 50 °C.

**Note S5: Optimization of the hybrid gripper design parameters**

To fabricate a functional gripper that can display well-organized pick-and-place tasks, we carefully optimized the design of gripper structures. We observed that the initially 3D printed gripper tips were over-stretched and -curved toward the outer direction when reaching equilibrium state in DI water at room temperature (Figure S3A&B) Thus, we updated the gripper designs by adding the center area (Figure S3C) that can hold the two tips stably with another function of a carrier for targets during the pick-and-place task (marked as yellow lines in Figure S3D). Furthermore, in order to integrate magnetic responsive ferrogel, we finally modified the gripper design to make the areas for precise injection of ferrogel as described in Figure S1.

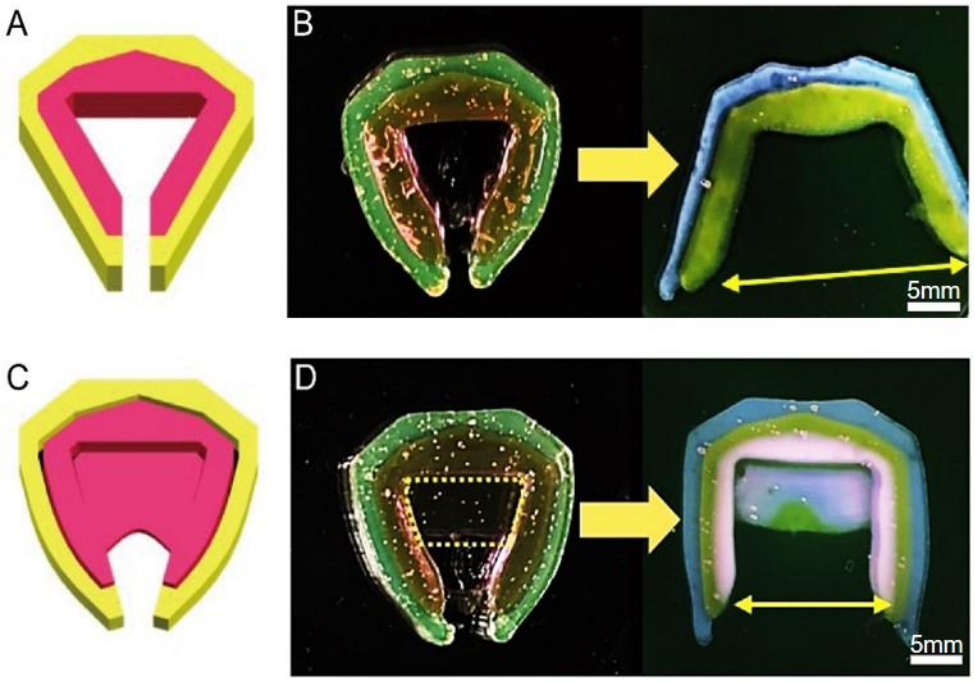


**Figure S3**. **Optimization of the hybrid gripper design. (A)** Schematic showing initial design of a gripper with no carrier structure at a center zone. **(B)** A 3D printed gripper displaying the unstably over widen tips at the equilibrium state in DI water. **(C)** Schematic showing updated design of a gripper with the carrier structure at the center zone. **(D)** A 3D printed gripper displaying the stably widen tips at the equilibrium state in DI water. Scale bars indicate 5 mm.

**Note S6: Experimental setup for ultrasonically responsive hybrid gripper**

The experimental setup for the characterization of both the temperature rise of the gripper and the tip-to-tip distance change under ultrasonic irradiation is shown in Figure S4. The photo of the experiment is shown in Figure S4A. The ultrasonic transducer was immobilized by a custom 3D printed holder placed at the bottom of the water tank. The hybrid hydrogel was placed on acoustically transparent PET film; the distance between the transducer and the hybrid hydrogel was fixed at 10 cm. The custom ultrasonic transducer was driven at its resonant frequency using a function generator (Tektronix AFG1022) connected to an RF amplifier (E & I 240L).

To measure the tip-to-tip distance under ultrasound irradiation (acoustic intensity of 253 $mW/cm^2$), the gripper was irradiated for 15 minutes intervals. Following the ultrasonic irradiation, the gripper was taken out from the water tank and the IR image and the photograph of the gripper were immediately taken (Figure S4B); the results from the experiment are summarized in Figure 3C.

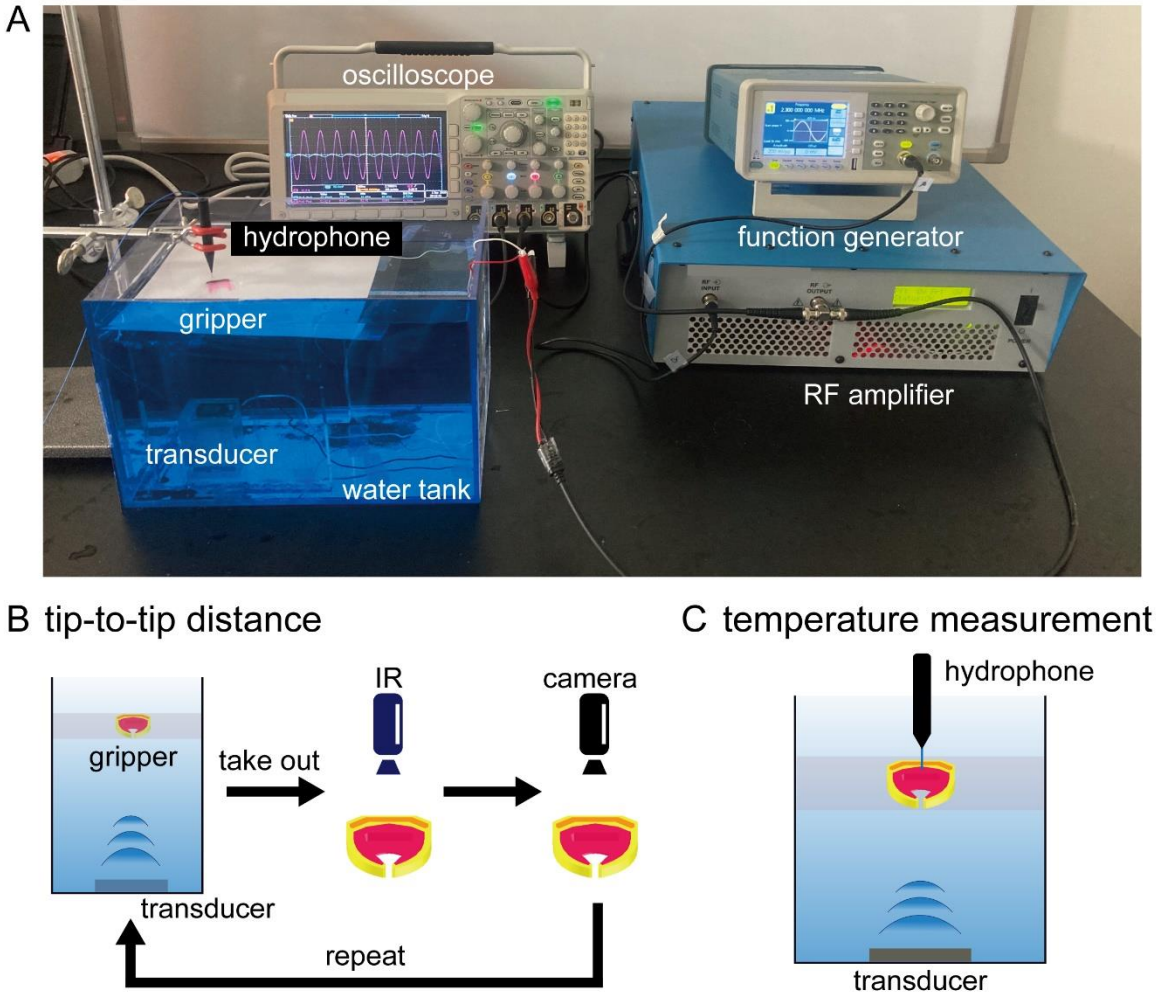


**Figure S4. The experimental setup for characterizing gripper's response to ultrasound. (A)** The photograph of the experimental setup. **(B)** The measurement process for the tip-to-tip distance. **(C)** The experimental setup for the temperature measurement at the gripper surface.

**Note S7: Characterization of ultrasound-mediated thermal response of hybrid gripper**

We used a simple bilayer structure for an ultrasound test. The thickness of the bilayer was 0.12 mm with 3 layers (4 mm per 1 layer). The ratio between the passive and active layers was 1:2. In this case, we used acoustic waves with an intensity of 95 mW/cm$^2$. We measured the curvature diameter of the bilayer. We used bilayer swelling ratio data previously tested by changing the temperature of the incubator for backtracking the temperature of the bilayer. The initial temperature was 24 °C, and it rose to 34 °C for 2 hours.

Second, we utilized our 3D gripper structure for the ultrasound test. In contrast to the former experiment, we used acoustic waves with an intensity of 100 mW/cm$^2$. In this case, we measured the angle between the legs of our gripper. Likewise, the gripper's incubator reference data was used for backtracking the temperature of the gripper. The initial temperature and the angle were 25 °C and 23 °, and it was changed up to 37 °C and 11 °, respectively.

To directly measure the temperature rise at the surface of the gripper, the fiber optics hydrophone was placed into the surface (~100 μm) of the stimuli responsive gel portion of the gripper (Figure S4C). Both the ultrasonic intensity and the temperature of the gripper surface was measured by a fiber optics hydrophone (FOH, Precision Acoustics, UK) connected to an oscilloscope (MDO3054, Tektronix). The pressure of the applied ultrasound was calculated by dividing the voltage output of the hydrophone ($V_{hp}$) by the hydrophone's sensitivity($S_{hp}$).

$$p = \frac{V_{hp}}{S_{hp}}$$

This pressure is converted to the average acoustic intensity as below equation (I: acoustic intensity [$W/m^2$], p: peak pressure [Pa], ρ: water density [$kg/m^3$], c: sound velocity in water [m/s]).

$$I = \frac{p^2}{2\rho \cdot c}$$

Figure S5 shows the change of temperature at the surface of the gripper under varying acoustic intensity. The heating rate was linearly proportional to the increasing the acoustic intensity increases as shown in Figure 3D.

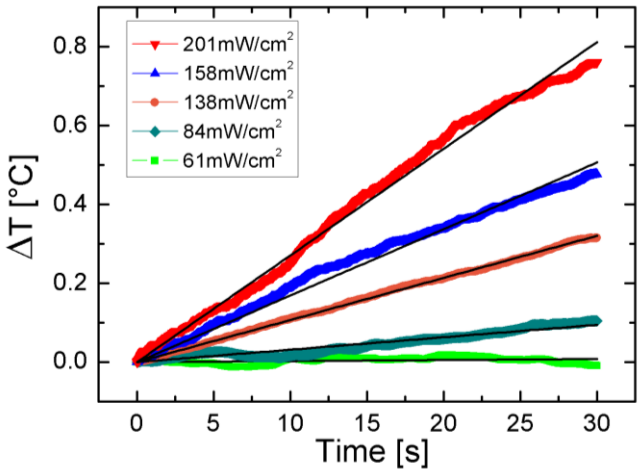


**Figure S5. The temperature rise as a function of ultrasonic irradiation intensity.**

**Note S8: Estimation of the attenuation coefficient of the NIPAM-based hydrogel**

The amount of heat of gripper can be expressed as below. For negligible temperature change (ΔT), the amount of heat is about 1.11 $\mathrm{mW/cm^2}$.

$$\mathrm{Q\ [mW/cm^2]} = C_s \frac{\partial T}{\partial t} + \frac{\Delta T}{R}$$

The attenuation coefficient of a gripper with an area of $1\,\mathrm{cm^2}$ receiving ultrasound can be calculated by the following equations.

$$\frac{Q}{P_{in}} = 1 - \frac{P_{out}}{P_{in}} = 1 - e^{-\alpha \cdot f \cdot t}$$

Followed the above process, the attenuation coefficient of the gripper is estimated to be approximately 1.5 dB/MHz cm, with the estimated interval between 1 to 2 dB/MHZ cm.

To elucidate the role of the layered-silicates (Laponite) inclusion, we measured temperature changes of the ultrasound responsive hydrogel as a function of weight percentage of the Laponite (Figure S6). The fiber optics hydrophone was placed on the surface of the ultrasound responsive hydrogel in a cuvette. The temperature change of the hydrogel with different Laponite loading concentrations was measured for 1000 seconds under the continuous ultrasonic irradiation. We observed that the relative temperature change of the hydrogel (normalized to the ultrasound responsive gel used in our study, 6.77 %) linearly increased as a function of weight percentage of the layered-silicates (Figure S6), thus indicating that the layered-silicates indeed act as scattering sites to thermalize the incoming ultrasound. We further observed that the ultrasound responsive hydrogel used in the gripper is about 8 times more effective in thermalizing the ultrasound compared to the non-silicates loaded NIPAM hydrogel (1 vs. 0.12). Moreover, we also confirm the possibility of further increasing the thermal response of the hydrogel through increasing the loading concentration, albeit it must be accompanied by suitable modifications of the printing conditions.

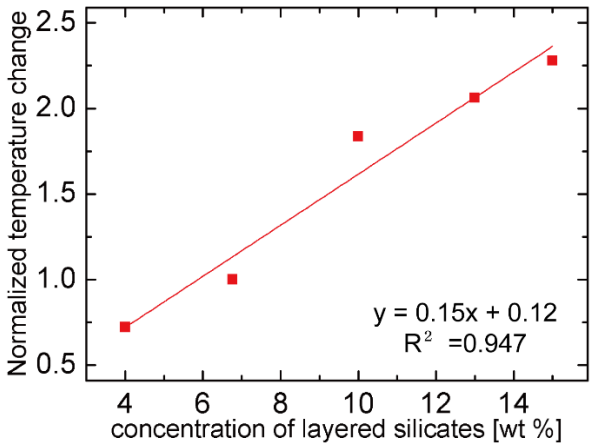


**Figure S6. Relative temperature change in ultrasound responsive hydrogel with different concentrations of layered-silicates. The temperature changes were normalized to the printed ultrasound responsive gel (6.77 %).**

The IR images of the gripper before/after the ultrasonic irradiation presented in Figure 3 of the main text shows a temperature reading of about 30 °C, which is lower than the typical LCST of the pNIPAM gel of around 32 °C. Although the IR images were only meant to be used in a qualitative manner, here we also present the IR image of the gripper and the matching photo directly taken out of the water tank under ultrasonic irradiation of 15 minutes. Although the short duration of the gripper being exposed to the ambient will cool down the surface, we observed that the surface temperature of the gripper is well above 32 °C, indicating that the ultrasonic induced heating can raise the temperature of the gel well above the LCST.

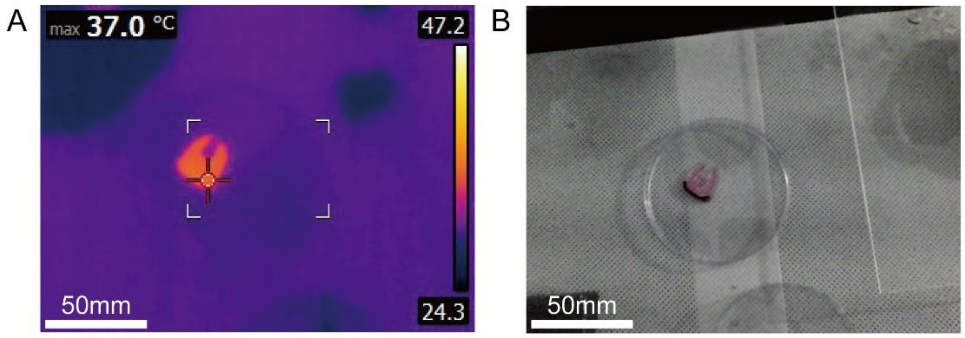


**Figure S7. 3D printed hybrid gripper with ultrasound for 15 minutes. (A)** The IR image of the gripper. **(B)** The optical image of the gripper.

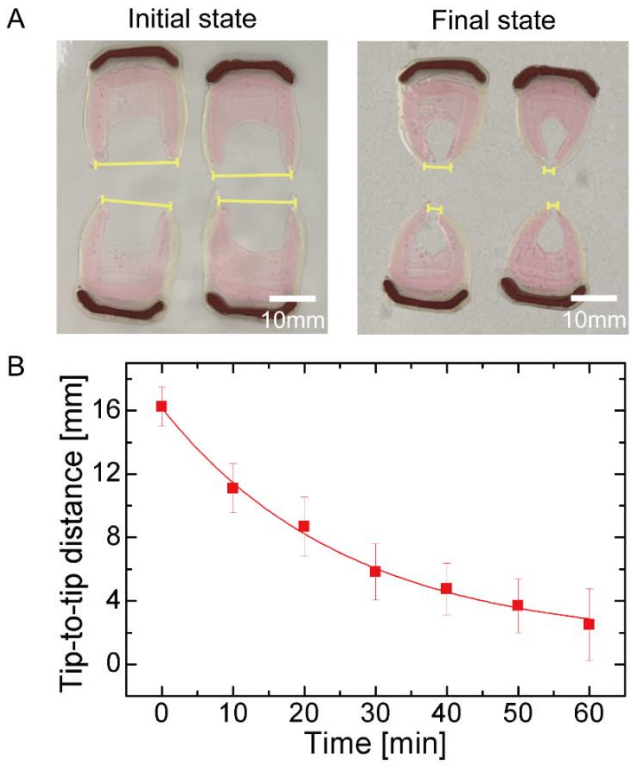


**Figure S8. Actuation of the hybrid grippers under ultrasound (A)** Results of initial state (time=0) and final state (time=60min). **(B)** Tip-to-tip distance as a function of time.

Furthermore, we verified the reproducibility and the consistency in ultrasonic actuation of the hydrogel grippers; the optical images of the four grippers before and after ultrasonic irradiation are shown in Figure S8 where a consistent shape transformation is clearly observed. The tip-to-tip distance of the grippers was measured as a function of time under ultrasonic irradiation (Figure S8B). In Figure S8B, the average tip-to-tip distance as a function of time and the standard deviation among the girppers show that all grippers follow the same trend where the tip-to-tip distance decreased exponentially. The consistency in both the fabrication and ultrasonic actuation of the gripper is clearly observed.

**Note S9: Pick-and-place task of the hybrid gripper**

Similarly, the experimental setup for the pick-and-place task is as in Figure S9 and the custom ultrasonic transducer setup is same as the experiment to measure the tip-to-tip distance. The maze composed of 3D printed walls on a PET sheet, on an acrylic support 10 cm above the bottom, was placed in a water tank. The salmon roe was placed on the target point and the gripper was placed at the starting point in the maze. The pick-and-place process is the same as Figure 4B-G, and neodymium magnets were used for the magnetic locomotion control. The camera was fixed directly above the maze and was recorded in video mode.

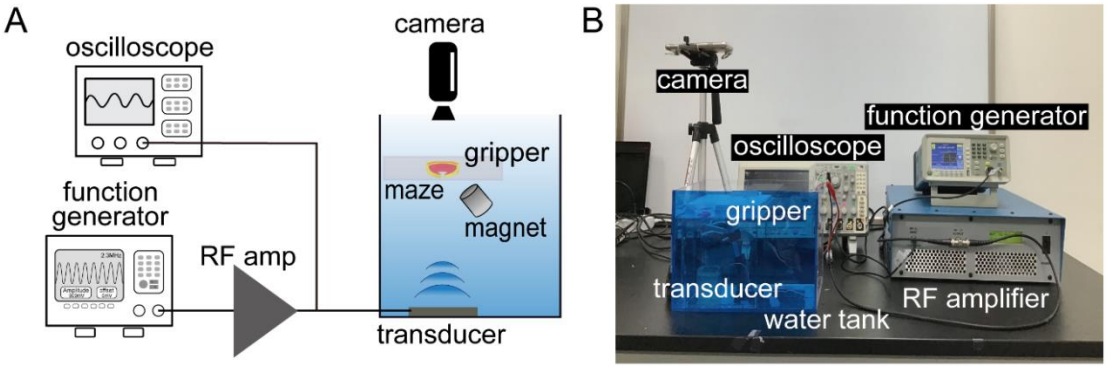


**Figure S9. The experimental setup for the pick-and-place task. (A)** Schematic illustration of the pick-and-place task. **(B)** Photograph of the pick-and-place task setup.

**Supplemetal Movie 1.** Pick-and-place task of hybrid gripper. The snap shots are in **Figure 4**.

## References


(1) Jiang, W.; Niu, D.; Liu, H.; Wang, C.; Zhao, T.; Yin, L.; Shi, Y.; Chen, B.; Ding, Y.; Lu, B. Photoresponsive Soft-Robotic Platform: Biomimetic Fabrication and Remote Actuation. *Adv. Funct. Mater.* **2014**, *24*, 7598–7604.

(2) Stoychev, G.; Turcaud, S.; Dunlop, J. W. C.; Ionov, L. Hierarchical Multi-Step Folding of Polymer Bilayers. *Adv. Funct. Mater.* **2013**, *23*, 2295–2300.

(3) Erol, O.; Pantula, A.; Liu, W.; Gracias, D. H. Transformer Hydrogels: A Review. *Advanced Materials Technologies* **2019**, *4*, 1900043.

(4) Sydney Gladman, A.; Matsumoto, E. A.; Nuzzo, R. G.; Mahadevan, L.; Lewis, J. A. Biomimetic 4D Printing. *Nat. Mater.* **2016**, *15*, 413-418.

(5) Ionov, L. 4D Biofabrication: Materials, Methods, and Applications. *Adv. Healthc. Mater.* **2018**, *7*, 1800412.

(6) Li, Y. C.; Zhang, Y. S.; Akpek, A.; Shin, S. R.; Khademhosseini, A. 4D Bioprinting: The next-Generation Technology for Biofabrication Enabled by Stimuli-Responsive Materials. *Biofabrication* **2017**, *9*, 012001.

(7) Tibbits, S. 4D Printing: Multi-Material Shape Change. *Archit. Des.* **2014**, *84*, 116-121.

(8) Liu, J.; Erol, O.; Pantula, A.; Liu, W.; Jiang, Z.; Kobayashi, K.; Chatterjee, D.; Hibino, N.; Romer, L. H.; Kang, S. H.; Nguyen, T. D.; Gracias, D. H. Dual-Gel 4D Printing of Bioinspired Tubes. *ACS Appl. Mater. Interfaces* **2019**, *11*, 8492–8498.

(9) Ding, Z.; Salim, A.; Ziaie, B. Squeeze-Film Hydrogel Deposition and Dry Micropatterning. *Anal. Chem.* **2010**, *82*, 3377-3382.

(10) Liu, J.; Erol, O.; Pantula, A.; Liu, W.; Jiang, Z.; Kobayashi, K.; Chatterjee, D.; Hibino, N.; Romer, L. H.; Kang, S. H.; Nguyen, T. D.; Gracias, D. H. Dual-Gel 4D Printing of Bioinspired Tubes. *ACS Appl. Mater. Interfaces* **2019**, *11*, 8492-8498.

(11) Schild, H. G. Poly(N-Isopropylacrylamide): Experiment, Theory and Application. *Progress in Polymer Science* **1992**, *17*, 163-249.

(12) Ahn, S.; Kasi, R. M.; Kim, S.-C.; Sharma, N.; Zhou, Y. Stimuli-Responsive Polymer Gels. *Soft Matter* **2008**, *4*, 1151-1157.